Intra-catchment variability of surface saturation – insights from long-term observations and simulations

Barbara Glaser[1,2], Marta Antonelli[3,1], Luisa Hopp[2], Julian Klaus[1]

[1]Catchment and Eco-Hydrology Research Group, Luxembourg Institute of Science and Technology, Esch/Alzette, 4362, Luxembourg
[2]Department of Hydrology, University of Bayreuth, Bayreuth, 95447, Germany
[3]Hydrology and Quantitative Water Management Group, Wageningen University & Research, Wageningen, 6700, The Netherlands

Correspondence to: Barbara Glaser (barbara.glaser@list.lu)

Abstract

The inundation of flood-prone areas varies in space and time and can have crucial impacts on runoff generation and water quality when the surface saturated areas become connected to the stream. In this study, we aimed to investigate and explain the variability of surface saturation patterns and dynamics within a forested headwater catchment. On the one hand, we mapped surface saturation in seven distinct riparian areas of the Weierbach catchment (Luxembourg) with thermal infrared images, taken weekly to bi-weekly over a period of two years. On the other hand, we simulated the surface saturation generation in the catchment with the integrated surface subsurface hydrologic model HydroGeoSphere over the same period. Both the observations and simulations showed that the saturation dynamics were similar across the catchment, but that small differences between the dynamics at different areas occurred. Moreover, the model reproduced the observed saturation patterns well for all seasonal and hydrologic conditions and at all investigated locations. Based on the observations and simulation results and the matches and mismatches between them, we concluded that the generation of surface saturation in the Weierbach catchment was largely controlled by exfiltration of groundwater into local depressions. However, we also illustrate that the entire variability of the patterns, dynamics and frequencies of surface saturation within the different riparian areas of the catchment can only result from additional controlling factors to microtopography and groundwater exfiltration, such as differing hysteretic behaviour, differing subsurface structures, or additional water sources.

1 Introduction

It is critical for flood risk assessment to understand where and when water is standing or flowing on the ground surface outside of perennial surface water bodies. When such surface saturated areas connect to the stream via overland flow, they also become crucial for runoff generation and water quality. In general, surface saturated areas arise from 1) water ponding on the surface due to exceedance of the infiltration capacity of unsaturated soil, 2) water ponding on impermeable surfaces or saturated soil, 3) water exfiltrating from the subsurface or, 4) stream water extending into the floodplain (e.g. Megahan and King, 1985). Over the past years and decades, various field studies mapped and analysed the spatial and temporal occurrence of surface saturation within different landscapes (e.g. Ambroise, 1986, 2016; Dunne et al., 1975; Gburek and Sharpley, 1998; Latron and Gallart, 2007; Silasari et al., 2017; Tanaka et al., 1988). From the field studies it is well recognized that surface saturation varies in space and time and that its appearance is affected by structural (e.g. topography) and dynamic factors (e.g. precipitation intensity, antecedent moisture). Yet there is limited understanding on how surface saturation evolves spatially and temporally between and within landscapes and how the interplay of different controlling factors and generation processes controls the spatio-temporal variability of surface saturation.

Spatially distributed and dynamic hydrological models are potential tools for analysing the generation and development of surface saturation in space and time. Such models allow a detailed investigation of surface saturation at any desired location and time that goes far beyond the information that can be gained by any field observation. Several simulation studies systematically assessed the influence of static and dynamic factors on the temporal evolution, connectivity, and spatial

5 distribution of surface saturation by performing virtual experiments with hillslope models (Ogden and Watts, 2000; Reaney et al., 2014) or by testing a range of terrain indices for predicting time-integrated saturation patterns (Güntner et al., 2004). Other studies relied on dynamic distributed and semi-distributed simulations for analysing connectivity of surface saturation in relation to wetness conditions and catchment runoff (Mengistu and Spence, 2016; Qu and Duffy, 2007; Weill et al., 2013). Weill et al. (2013) and Partington et al. (2013) analysed the processes and water sources that generate surface saturation in a

10 wetland and a pre-alpine grassland headwater, respectively. Both studies applied a model belonging to the group of integrated surface-subsurface hydrologic models (ISSHMs, Sebben et al., 2013), which can simulate the interplay of different surface and subsurface processes of surface saturation generation (e.g. ponding of precipitation from the surface, exfiltration from the subsurface). Modelling studies that focus on a comprehensive spatio-temporal analysis of surface saturation dynamics within a landscape by evaluating the spatially distributed model outputs rather than aggregating the outputs are scarce (e.g. Nippgen

15 et al. (2015) for subsurface saturated areas)

When complementing field observations with simulations to analyse the generation and development of surface saturation in space and time, it is important to ensure that the model yields realistic results. Glaser et al. (2016) demonstrated for a small riparian area that a good match between modelled and observed discharge or soil moisture does not automatically imply a realistic simulation of saturation patterns. They concluded that a spatial validation of the dynamic saturation patterns itself is

20 crucial. However, only few of the existing modelling studies explicitly checked the realism of their simulated surface saturation with field observations before using them for further analyses. These studies focussed either on temporally integrated spatial patterns (Grabs et al., 2009; Güntner et al., 2004) or on temporal dynamics of overall catchment saturation (Birkel et al., 2010; Mengistu and Spence, 2016), but barely any study combined the observation and simulation of both surface saturation patterns and dynamics (Ali et al., 2014; Glaser et al., 2016). The lack of such studies is certainly explainable by the resources that are

25 necessary for obtaining appropriate field data. Today, we still lack a standard method to map surface saturation and the different existing methods such as the 'squishy boot' method, the usage of 'on-off' surface saturation sensors, the mapping of soil morphology or vegetation as surrogates, or the usage of remote sensing techniques (e.g. Dunne et al., 1975; Gburek and Sharpley, 1998; Güntner et al., 2004; Latron and Gallart, 2007; Mengistu and Spence, 2016; Silasari et al., 2017) all have their own advantages and disadvantages.

30 A relatively new and powerful method for mapping surface saturation is thermal infrared (TIR) imagery. TIR mapping relies on the difference between the surface temperature of water and other materials for identifying surface saturation. Previous work showed that recurrent mapping of surface saturation with high spatial resolution is possible with TIR imagery (Glaser et al., 2016; Pfister et al., 2010). Glaser et al. (2018) and Antonelli et al. (2019) applied TIR imagery mapping in the 42 ha forested Weierbach catchment in western Luxembourg and monitored the dynamics of surface saturation within several distinct

35 riparian areas along the Weierbach stream with a weekly to biweekly mapping frequency over several seasons.

In this study, we explore the intra-catchment variability of temporal and spatial characteristics of surface saturation (dynamics, frequencies, patterns) with a combination of field observation and modelling. We perform the study in the Weierbach catchment, where we can rely on existing TIR imagery data (Antonelli et al., 2019; cf. Glaser et al., 2018) and on previous modelling work for a 6 ha headwater of the catchment (Glaser et al., 2016, 2019) with the ISSHM HydroGeoSphere. Glaser

40 et al. (2016, 2019) simulated the 6 ha area of the catchment by accounting for a layering of the subsurface, while spatial heterogeneity was only represented by microtopography and by a different sequence of subsurface layers in the riparian zone compared to the hillslopes and plateau. Here, we extend the model setup to the entire 42 ha catchment without introducing additional heterogeneity and without performing a re-calibration. We simulate surface saturation in the catchment and contrast

the results with the observed saturation patterns from the TIR imagery, focussing on the long-term saturation dynamics over different seasons and wetness conditions (25 months with weekly to biweekly mapping resolution) and the spatial patterns of surface saturation occurrence and frequency at seven different riparian areas across the catchment. The two research objectives that we aim to address with this approach are:

1) How variable are surface saturation dynamics and patterns within a catchment and to what extent can we reproduce the variability of the saturation characteristics (dynamics, frequencies, patterns) with a rather homogenously set-up ISSHM?

2) What do we learn about the reasons for the intra-catchment variability of surface saturation characteristics from the matches and mismatches between simulation results and observations?

2 Study site and data

2.1 Physiography, climate and hydrometry

The Weierbach catchment is an intensively studied headwater catchment (42 ha) in western Luxembourg. About half of the catchment area is characterized by gentle slopes <5°, forming a plateau landscape unit (Martínez-Carreras et al., 2016). The rest of the catchment is characterized by hillslopes with slopes > 5°, forming a central V-shaped stream valley from north to south and a V-shaped tributary valley in the east. A third, few metres long stream branch is situated in the west of the central stream valley. Riparian zones along the stream account for 1.2 % of the catchment area (Antonelli et al., 2019). Large parts of the catchment are forested with deciduous trees (mainly European beech and Sessile oaks), the south-east and some other small parts are forested with conifers (mainly Norway spruce and Douglas spruce). The riparian zones are free of tree canopy and covered with ferns, moss, and herbaceous plants. Soil developed from Pleistocene Periglacial Slope Deposits as shallow and highly-permeable siltic, sceletic Cambisol with a depth ranging between 0.4 and 0.9 m (Gourdol et al., 2018; Juilleret et al., 2011; Moragues-Quiroga et al., 2017). Beneath the solum, a 0.5 – 1 m thick basal layer with bedrock clasts oriented parallel to the slope overlies fractured Devonian slate and phyllites (Gourdol et al., 2018; Juilleret et al., 2011; Moragues-Quiroga et al., 2017; Scaini et al., 2017). In the riparian zones, soil and basal layer have been eroded and the fractured bedrock is overlain by shallow organic Leptosols (Glaser et al., 2016).

The climate is oceanic-continental without apparent seasonality in precipitation and with negligible amounts of snow (Carrer et al., 2019). Mean annual precipitation during the period from October 2013 to September 2017 was 955±53 mm. Mean annual discharge was 546±253 mm, with exceptionally dry conditions in the hydrological year 2017. During wet periods, discharge is characterized by double peak hydrographs with first peaks appearing as immediate response to precipitation and second pronounced peaks appearing 48h to 72h later (cf. Martínez-Carreras et al., 2016). During dry periods, only first hydrograph peaks occur and the stream dries out intermittently starting from the source areas downstream.

Hydrological and meteorological data that were used in this study were measured from October 2013 to January 2018. Data from the period from October 2013 to September 2015 were used for spin-up simulations, data from the period from October 2015 to January 2018 were used to drive and validate the actual simulation (cf. Section 3). Discharge was measured with water pressure transducers (ISCO 4120 Flow Logger, 15 min logging intervals) at four v-notches installed at the outlet of the catchment (SW1, Fig.1) and upstream of the confluences of the three branches (SW2-SW4). Groundwater levels were continuously recorded every 15 minutes with pressure sensors (OTT CTD) in five piezometers installed in different landscape units (riparian zone, hillslope, plateau) of the catchment (Fig. 1, GW1-3, GW5, GW7). Soil moisture was continuously monitored (30 min logging intervals) with water content reflectometers (CS650, Campbell Scientific) installed horizontally in 10, 20, 40 and 60 cm depth at four different sites (Fig.1, SM3-5, SM7). At each site, two depth profiles were monitored. In addition, soil moisture in 10 cm depth was monitored with water content reflectometers (CS616, Campbell Scientific, 30 min logging intervals) at five locations crosscutting the riparian zone of the stream source area of the middle stream branch (Fig. 1, SSM1-5).

Cumulative precipitation was recorded every 5 minutes with a tipping bucket raingauge (Young 52203, unheated, 1 m height) at an open area within the catchment (data gaps were filled ~~by estimating~~ a linear regression to data from a station approximately 4.5 km southward). Potential reference evapotranspiration was estimated based on measured air temperature, relative humidity, wind speed, and net radiation according to the FAO Penman-Monteith formulation (Allen et al., 1998). Air

5   temperature and relative humidity data were recorded next to the soil moisture profile SM5 (Fig. 1, HMP45C-LC, Campbell Scientific, 15 min logging intervals, 2 m height). Wind speed and radiation data were recorded approximately 4.5 km southward of the study site. Wind speed (Young Wind Monitor 05103, Vector A100R Anemometer) was recorded every 15 minutes ~~in~~ 3 m height and converted to wind speed in 2 m height (data gaps closed with data from a station approximately 11.5 km north-eastward) following the FAO guidelines (Allen et al., 1998). Net radiation was recorded every 15 minutes (Kipp

10 & Zonen NR Lite net radiometer) until May 2017. From June 2017 on (and for closing other data gaps), we used net radiation data recorded every 5 minutes close to Luxembourg Airport (~40 km southeast of the study site), as these measurements were highly correlated (linear regression with an intercept of 7.6 W m^{-2}, a slope of 0.92, $R^2 = 0.81$) with the measurements close to the study site in the years before.
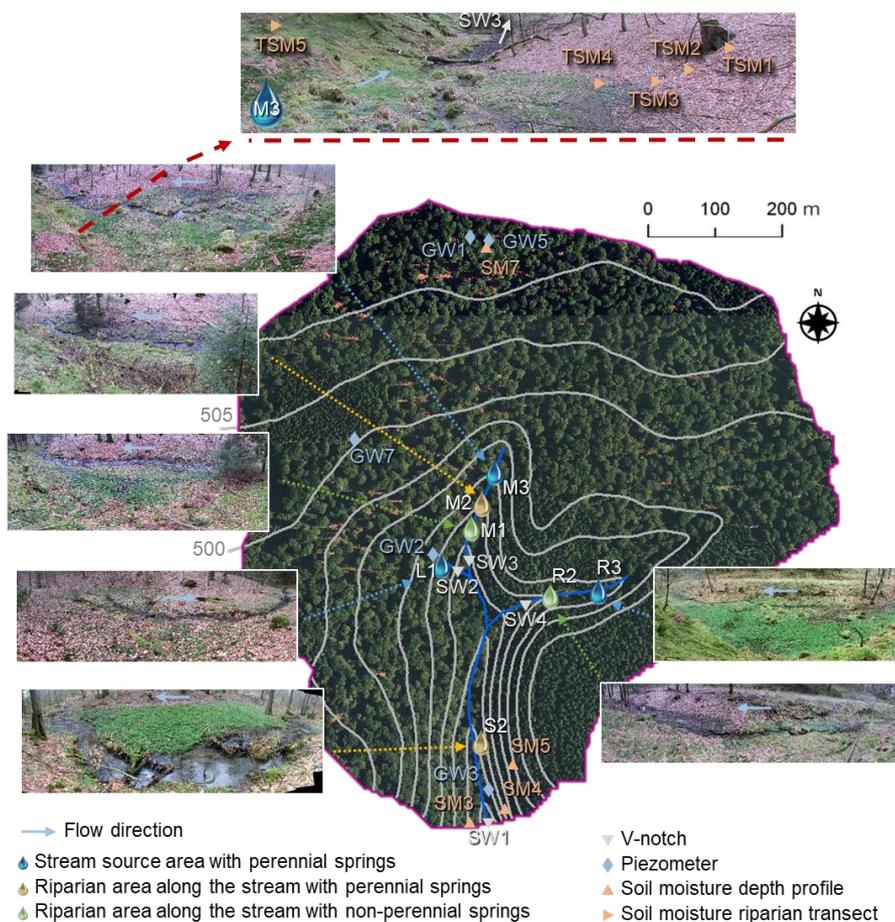
Figure 1: The Weierbach catchment with the locations of the installed v-notches, piezometers, soil moisture sensors and the seven investigated riparian areas.

2.2 Surface saturation

Here, we define surfaces as saturated as soon as water is standing or flowing on the ground surface (Glaser et al., 2018). This involves water bodies such as lakes and streams, but excludes mere saturation in the topsoil. According to this definition, surface saturation in the Weierbach catchment generally only occurs in the streambed and the adjacent riparian zones. Other

5 areas that were occasionally observed to be surface saturated during very wet conditions or 'rain on snow' events are forest roads and the prolongation of the streambed above the source regions into the hillslopes. We focus in this study on seven distinct riparian areas in the catchment, which can be classified into three different categories (cf. Antonelli et al., 2019): i) stream source areas with perennial springs (L1, M3, R3, blue areas Fig. 1), ii) areas along the stream with perennial springs (M2, S2, yellow areas Fig. 1), and iii) areas along the stream with non-perennial springs (M1, R2, green areas Fig.1).

10 We mapped the surface saturation in these seven riparian areas weekly to biweekly from November 2015 to December 2017 with thermal infrared imagery (TIR). Details on the identification of surface saturation with TIR imagery and on the collected surface saturation dataset are presented and discussed in Glaser et al. (2018) and Antonelli et al. (2019). In brief, we created panoramic TIR images of the distinct areas and identified the locations of surface saturation (including the stream) within the images. To do this, each pixel in an image was assigned to be saturated or unsaturated based on the temperature range of

15 locations that were obvious to be saturated from field observations and visual images. In case the contrast between water temperature and temperature of surrounding materials was not sufficient for a reliable pixel classification, the images were excluded from the analysis. In case the pixel classification was affected by a poor temperature contrast or by pixels representing vegetation or snow cover in the images, the images were analysed but flagged as less reliable. Altogether, we obtained 291 binary panoramic images showing the temporal dynamics of surface saturation patterns in the seven studied riparian areas with

20 total numbers of images per site ranging between 34 (L1) and 48 (M2).

Time series of saturation were created for each area by accounting for the percentage of saturated pixels within the individual panoramic images. We normalized the saturation percentages to the maximum observed percentage of saturation in the distinct areas in order to allow a comparison of the saturation dynamics between the different riparian areas. For picturing the spatial surface saturation dynamics within a distinct riparian area, we created maps of saturation frequency. We counted for each area

25 how often the individual pixels of the panoramic TIR images were classified as saturated and normalized the resulting frequency numbers by the total number of TIR images analysed for that area.

The resulting maps of normalized saturation frequency rarely showed pixels that were always saturated (i.e. reaching a normalized frequency of 1). In reality, surface saturation was more persistent than indicated by the frequency maps. The reason for this artefact is that the perspective of the individual TIR panoramas was not 100% identical for all mapping instances and

30 that vegetation sometimes covered parts of the saturated surface, especially during near dry conditions. We co-registered the individual panoramas against a reference panorama for each area, but slight position shifts were inevitable. As a result, the images that were placed on top of each other did not always overlap exactly and the generated saturation frequency maps are blurred. Nonetheless, the maps of normalized saturation frequencies are very useful to understand at a glance where surface saturation occurs more and less frequent within an area and to be used for model validation.

3 Catchment model

3.1 Model setup and parameterisation

We simulated the spatio-temporal dynamics of surface saturation across the Weierbach catchment with HydroGeoSphere (HGS, Aquanty Inc.). HGS is an integrated surface subsurface hydrological model and allows simultaneous simulation of transient surface and subsurface flow. Subsurface flow is simulated based on the 3D Richards equation. Surface flow is

40 simulated based on the diffusive-wave approximation of the 2D Saint Venant equation. Evapotranspiration is simulated with a comparatively simple approach, following the mechanistic concept of Kristensen and Jensen (1975). The equations are

linearized implicitly using the Newton-Raphson approach and solved in an unstructured finite element grid. HGS has been used in the past for addressing diverse questions at various temporal and spatial scales (e.g. Ala-aho et al., 2015; Davison et al., 2018; Erler et al., 2019; Frei et al., 2010; Munz et al., 2017; Nasta et al., 2019; Partington et al., 2013; Schilling et al., 2017; Tang et al., 2018). It also has already been applied for a 6 ha headwater region of the Weierbach catchment (Glaser et

5   al., 2016, 2019). In this study, we applied the parameterization of Glaser et al. (2016) to the entire 42 ha catchment without performing an additional parameter calibration.

The catchment was spatially discretized into 42,274 triangular elements, using the mesh generator AlgoMesh (HydroAlgorithmics Pty Ltd). Edge lengths of the mesh elements ranged from > 30 m at the plateau to < 0.4 m for the seven analysed riparian zones and the streambed (Fig. 2). It was crucial to use such a fine mesh resolution in the riparian zone in

10   order to enable a comparable spatial detail as obtained with the TIR imagery for the surface saturation patterns. Vertically, the model grid comprised 5 m, which were divided into 14 layers with element depths ranging from 0.15 m for the top layers to 0.5 m for the bottom layers (Fig. 2).
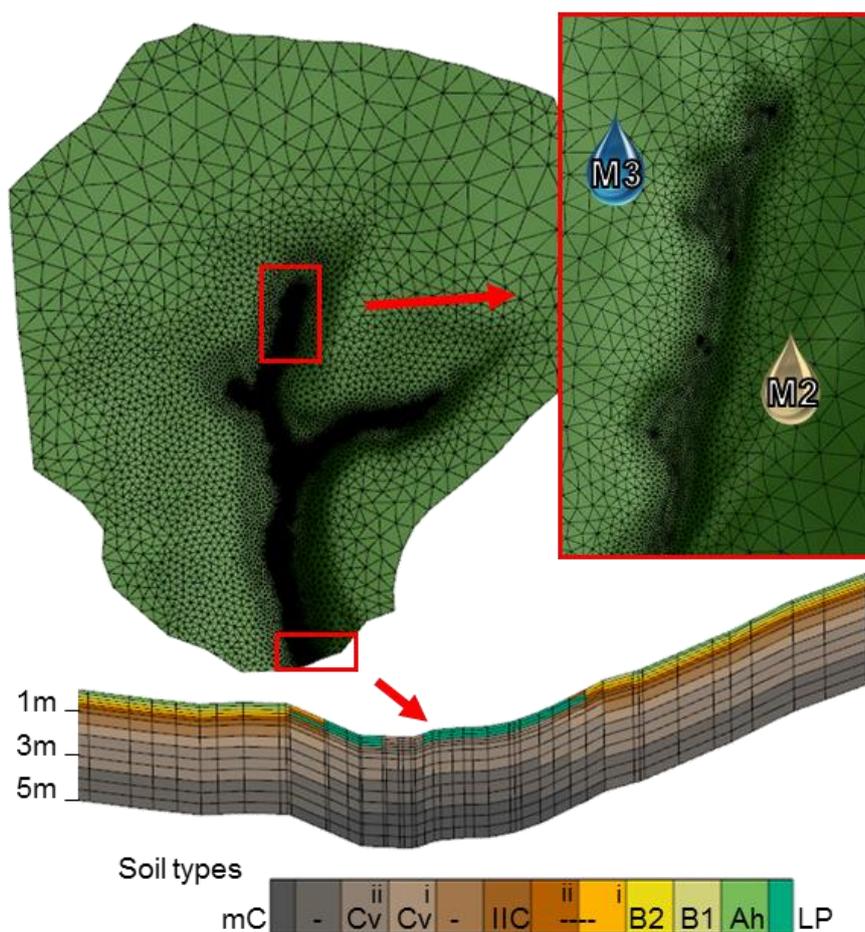
15   **Figure 2: Setup of the model mesh with a zoom on the fine horizontal resolution in the riparian areas and the streambed (inset on the right) and a vertical cross section through the stream valley and adjacent hillslopes (bottom) showing the vertical discretization and assignment of different soil properties (cf. Tab. 1). Ah = topsoil, B1 and B2 =subsoil, IIC = basal layer, Cv = fractured bedrock, Cm = fresh bedrock.**

The subsurface was parameterized homogeneously with 10 different property layers, representing top- and subsoil (Ah, B1, B2), the basal layer (IIC), fractured and fresh bedrock (Cv, Cm), and layers of transition between subsoil, basal layer, and fractured bedrock (Fig. 2). We implemented spatial heterogeneity in the stream valleys, where soil and basal layer were eroded and the outcropping fractured bedrock was overlain with organic, stagnic Leptosol in the riparian zones (Fig. 2). We used the

5 Mualem-van Genuchten soil hydraulic functions for describing the saturation-pressure relation. The necessary soil hydraulic parameter values for the different property layers (porosity, residual saturation, van Genuchten α, van Genuchten β, saturated hydraulic conductivity, Tab. 1) were assigned according to Glaser et al. (2016). We only parameterised one additional layer for the fractured bedrock (Cv (ii)) in order to account for the adapted depth of 5 m in the catchment model compared to the depth of 3 m in the headwater model.

Table 1: Soil hydraulic parameters of the different soil property zones. Table adapted from Glaser et al. (2016)

Soil property zone	Residual saturation	van Genuchten parameter α [m^{-1}]	van Genuchten parameter β	Porosity	Saturated hydraulic conductivity [m d^{-1}]
Ah	0.12	6.6	1.46	0.74	1.71E+01
B1	0.10	22.1	1.42	0.61	1.71E+01
B2	0.10	22.1	1.42	0.45	4.59E+01
B2-IIC (i)	0.10	22.1	1.42	0.3	9.30E+02
B2-IIC (ii)	0.10	22.1	1.42	0.15	2.04E+03
IIC	0.02	6.0	1.50	0.20	8.40E+02
IIC-Cv	0.02	6.0	1.50	0.15	3.00E+00
Cv (i)	0.02	6.0	1.50	0.10	1.20E-02
Cv (ii)	0.02	6.0	1.50	0.07	1.20E-02
Cv-mC	0.02	6.0	1.50	0.05	9.00E-04
mC	0.02	6.0	1.50	0.01	2.40E-05
LP	0.10	22.1	1.42	0.61	7.80E+00

Surface and subsurface flow were coupled via a Darcy flux exchange through a thin coupling layer (10^{-4} m). We assumed different Manning's surface roughness values for the forested area (1.24*10^{-6} d m$^{-1/3}$), the riparian zone (9.41*10^{-7} d m$^{-1/3}$),

15 and the stream bed (4.4*10^{-7} d m$^{-1/3}$) (cf. Glaser et al., 2016). Evapotranspiration properties (Tab. S1) were assigned individually for the deciduous forest, the coniferous forest in the southeast of the catchment, and the riparian zones including the streambed and values were based on the calibrated values of Glaser et al. (2016). The simulation was driven with daily sums of precipitation and reference evapotranspiration, which were treated as being spatially uniform. The outer edge of the surface domain was assigned as critical depth boundary, allowing water to leave the model domain via surface flow. Side and

20 bottom boundaries of the subsurface domain were no flow boundaries. A spin-up simulation drained the catchment from full saturation to steady state conditions (for 1 mm d^{-1} of precipitation, no evapotranspiration) and subsequently repeated the period from October 2013 to October 2015 three times for obtaining realistic initial conditions. The actual simulation spanned over the period from October 2015 to January 2018, the period where we mapped surface saturation with TIR imagery.

3.2 Assessment of model performance

25 We benchmarked the model against measured discharge, groundwater level, soil moisture, and surface saturation patterns and dynamics at various locations (Fig. 1). We calculated the Kling Gupta Efficiency (KGE) as a combined measure for correlation, bias, and relative variability (Gupta et al., 2009) between simulated and observed discharge. We also calculated KGEs for the simulated groundwater levels, but particularly evaluated the groundwater level dynamics rather than absolute values based on

Pearson correlation coefficients. Soil moisture was also evaluated based on its dynamics with Pearson correlation coefficients, while absolute values were only compared visually. Since simulated soil moisture was extracted from model nodes whose depths did not exactly correspond with the measurement depths, we interpolated depth-weighted average values from the model output for calculating the correlation with the observations in the respective depths. The interpolated model values of

5   volumetric water content were then correlated with the observations of water content, averaging the measurements of the twin depth profiles at the monitoring sites.

For comparing the simulation output with the surface saturation information obtained with the TIR images, it was necessary to convert the model output into a comparable format via several processing steps: First, we extracted the surface water depths in the surface domain of the model for noon of the days where TIR images were taken and analysed. Next, we transformed the

10   surface water depths into a binary saturation map of the entire catchment by classifying the surface domain cells as saturated if water depths were $>10^{-4}$ m. The depth of 10^{-4} m corresponds to the penetration depth of the used TIR camera for water columns and thus is the minimum depth that could be detected as pure water temperature signal with the camera. Finally, we projected the model output into jpeg images with the same perspective and extent of the TIR panoramic images by turning, bending, and cutting the modelled saturation maps according to each of the seven riparian areas individually. This model

15   output processing allowed us to perform the same calculations for the model output as for the TIR images, i.e. to create time series of normalized saturation and maps of normalized saturation frequencies for the seven riparian areas with comparable perspectives and extents. Since it was not possible to project the model output identically to the perspectives of the TIR images, we compared the saturation dynamics and patterns of the model images with the observations qualitatively (visually) only. A quantitative comparison would have been biased by differences in image distortions and total area extent.

20   Furthermore, we compared the simulated frequency of surface saturation with the simulated frequency of groundwater reaching the surface. To do this, we marked the surface cells below which the subsurface domain was fully saturated from the bottom to the surface as cells where groundwater reached the surface. This binary information was transformed into a frequency map analogous to the procedure for creating the surface saturation frequency maps, using the same output times.

4 Results

4.1 Simulation of discharge, groundwater level and soil moisture

The model reproduced the seasonal dynamics of measured discharge very well (Fig. 3, Fig. S1). The best fit was obtained at the outlet (SW1) with a KGE of 0.74. Discharge at SW2, SW3, and SW4 was reproduced equally well with KGEs of 0.49, 0.48, and 0.47. Groundwater levels were captured well with the model at the locations close to the riparian zone (KGE=0.57, r=0.78 for GW2; KGE=0.64, r=0.84 for GW3). At hillslopes and plateau, simulated groundwater levels were similar to the

30   observed levels during the wet season, but during dry conditions the groundwater levels did not fall deep enough (Fig. 3, Fig. S1). This level discrepancy was reflected in low KGEs (0.30 for GW1, 0.21 for GW5, 0.02 for GW7). However, general dynamics of level increasing and decreasing were also captured at hillslopes and plateau (r = 0.66 for GW5, r = 0.62 for GW7, and r = 0.76 for GW1; note that the value for GW1 only includes data for wet periods, since the piezometer fell dry during summer months).

35   Simulated soil moisture generally showed a transition from higher to lower responsiveness from topsoil to subsoil layers consistent with the monitored soil moisture (Fig. 3, Fig. S1) and Pearson correlation coefficients indicated overall a good agreement between simulated and observed soil moisture dynamics (Tab. 1). As for the groundwater levels at the hillslopes and plateau, soil moisture observations showed a distinct decrease in water content during dry periods, which the simulation could not reproduce to the same extent. The observed water content in the riparian zone was always close to saturation (TSM4,

40   Fig. 3), while the simulation showed a decrease in water content during dry periods in the riparian zone. Yet the simulation also showed a spatial trend for more permanent soil saturation in the riparian zone (TSM4) and its vicinity (TSM3, Fig. S1)

than at the hillslopes and plateau. The simulated values of water content were similar to the observed values at some locations (e.g. TSM2, SM4, Fig. 3) and clearly differed at other locations (e.g. SM7, Fig. 3), but the matches and mismatches of the volumetric water content did not clearly depend on specific areas or landscape units. Moreover, we think that moisture dynamics and responsiveness are more informative for model performance than the absolute water content values, since also

5   the measured values of volumetric water content differed ~~from each other~~ within small distances (e.g. measurements of water content in 10 cm depth at profile SM7, Fig. 3).
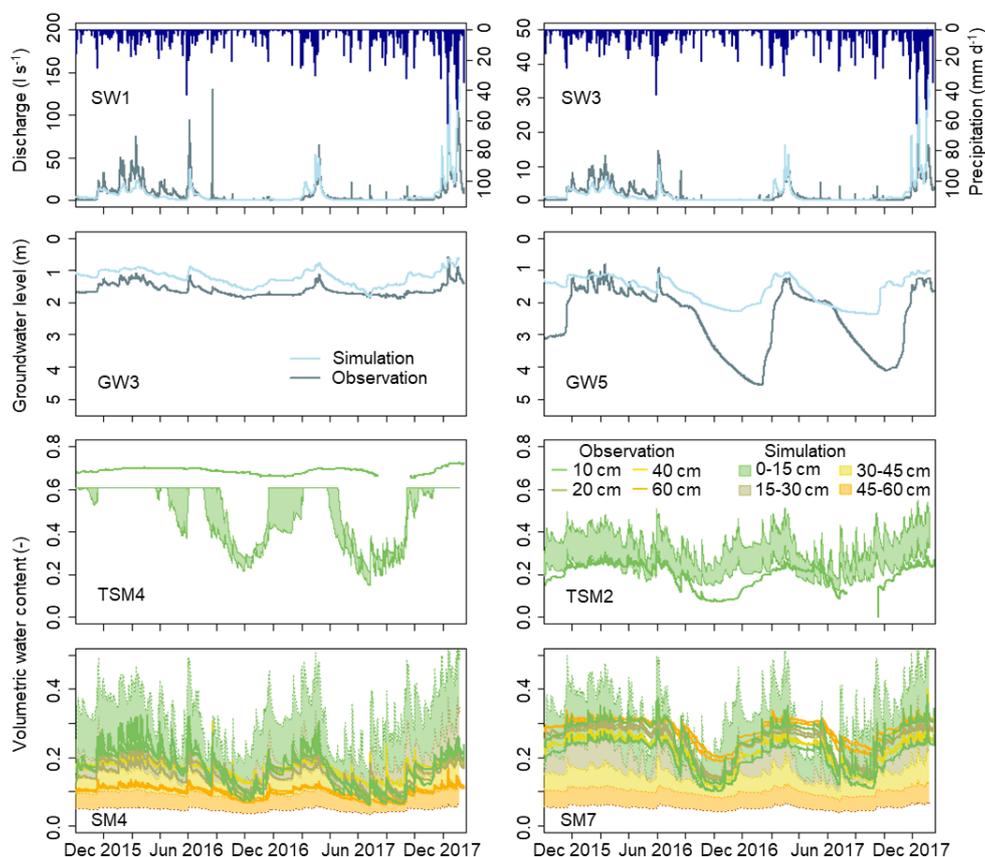
Figure 3: Simulated and observed time series of discharge, groundwater level below the surface, and volumetric water content.
10 **Colour bands indicate the possible span of simulated volumetric water contents in the depths between two model nodes. The time series of the observation locations (cf. Figure 1) that are not shown here, are shown in the supplemental material (Figure S1).**

Table 2: ~~Coefficients of~~ Pearson correlation between simulated and observed volumetric water content of the soil for the different measurement locations and depths (cf. Fig. 1).

	SM3	SM4	SM5	SM7	TSM1	TSM2	TSM3	TSM4	TSM5
10 cm	0.54	0.75	0.70	0.59	0.60	0.62	0.67	0.30	0.85
20 cm	0.67	0.82	0.76	0.62					
40 cm	0.82	0.89	0.88	0.79					
60 cm	0.85	0.92	0.91	0.82					

4.2. Dynamics of surface saturation

The observed dynamics of normalized surface saturation (Fig. 4, coloured lines) were similar for all seven investigated riparian areas and followed the seasonal trend of the ~~catchment~~ discharge. Yet some differences between the studied areas were discernible. For example, saturation was less persistent between February and April 2016 in the two areas without perennial

5 springs (M1, R2, Fig. 4) than in the other areas. Maximum saturation was reached in December 2017 at M1, R2 and S2, but between February and April 2016 at the other locations (Fig. 4). ~~As for~~ the observations, the simulated dynamics of normalized surface saturation (Fig 4, black lines) followed the general trend of the simulated discharge dynamic. The simulation showed a faster decrease and increase of the normalized saturation during dry periods than ~~it~~ was observed in most areas. However, simulated discharge also seemed to decrease and increase earlier than it was observed (c.f. Section 4.3). The simulated

10 saturation dynamics did not clearly differ between the different locations and thus behaved more synchronous than the observations (e.g. maximum simulated saturation in December 2017 in all areas). As a result, the match between simulated and observed dynamics of normalized saturation was better for some areas (e.g. M1, R2, Fig. 4) than for others (e.g. S2, L1, Fig. 4).

The dynamic changes of normalized simulated saturation matched the normalized observations generally well, despite ~~of~~

15 under- and over-estimat~~ed amounts~~ of minimum and maximum absolute saturation for all areas. The minimum ~~amount~~ of saturated pixels in the TIR panoramas ranged between 0.02 % at M3 and R3 and 3.38 % at S2, while the model did not simulate any surface saturation during the driest period (Fig. 4). In addition, simulated normalized saturation stayed longer close to the minimum than the observed saturation for several areas (L1, S2, M1). These results show that the model simulated a stronger dry-out than observed in the Weierbach. At the same time, the simulation overestimated maximum saturation in the riparian

20 zone (Fig. 4). The overestimation was not equally strong at the seven investigated areas and as a result, the distinction between areas ~~showing~~ higher or lower maximum saturation was not the same for observation and simulation (e.g. R3 showing one of the highest maximum saturation in the observation, but one of the lowest maximum saturation in the simulation compared to the other areas).

4.3 Discharge – surface saturation relationship

25 The Pearson correlation between normalized saturation and discharge at the outlet SW1 was > 0.65 for both the simulation and the observation in almost all riparian areas. L1 was the only exception with $r_{obs} = 0.54$ (Fig. 5). The simulated relationships between normalized saturation and discharge resembled the observed relationships in terms of value range and shape (Fig. 5), although the observation data ~~scattered~~ distinctly more than the simulation data. A power law relationship approximated the observed relationship between discharge and saturation for all seven areas, when data that were taken during rainfall or rising

30 discharge were excluded (cf. Antonelli et al., 2019). For some areas, the simulation matched the trend lines of the observation data closely (e.g. L1, M2). For other areas, the visual fit of the model output to the observation data was less good (e.g. S2, R3), but still described a similar trend.

Despite the common shape of a power law function, the saturation – discharge relationships were slightly different between the different areas, both for observation and simulation data. For example, the power law functions fitted to the observations

35 showed that saturation during high flow conditions (> 5 l s⁻¹) increased most strongly with discharge in the sources areas (especially M3 and R3). During low flow conditions (< 1 l s⁻¹), the source areas (L1, M3, R3) showed the lowest amount of normalized saturation and the least change relative to discharge compared to the other areas. In the simulated relationships, the increase in saturation for high discharge (> 5 l s⁻¹) was strongest for M3 and S2. The simulated relationship between discharge and surface saturation during low flow (< 1 l s⁻¹) was similar for all areas in terms of slope, but differed in the amount

40 of normalized saturation, being highest for areas in the east stream ~~branch~~ (R2, R3), followed by the middle upstream ~~branch~~ (M1, M2, M3), and L1 and S2.
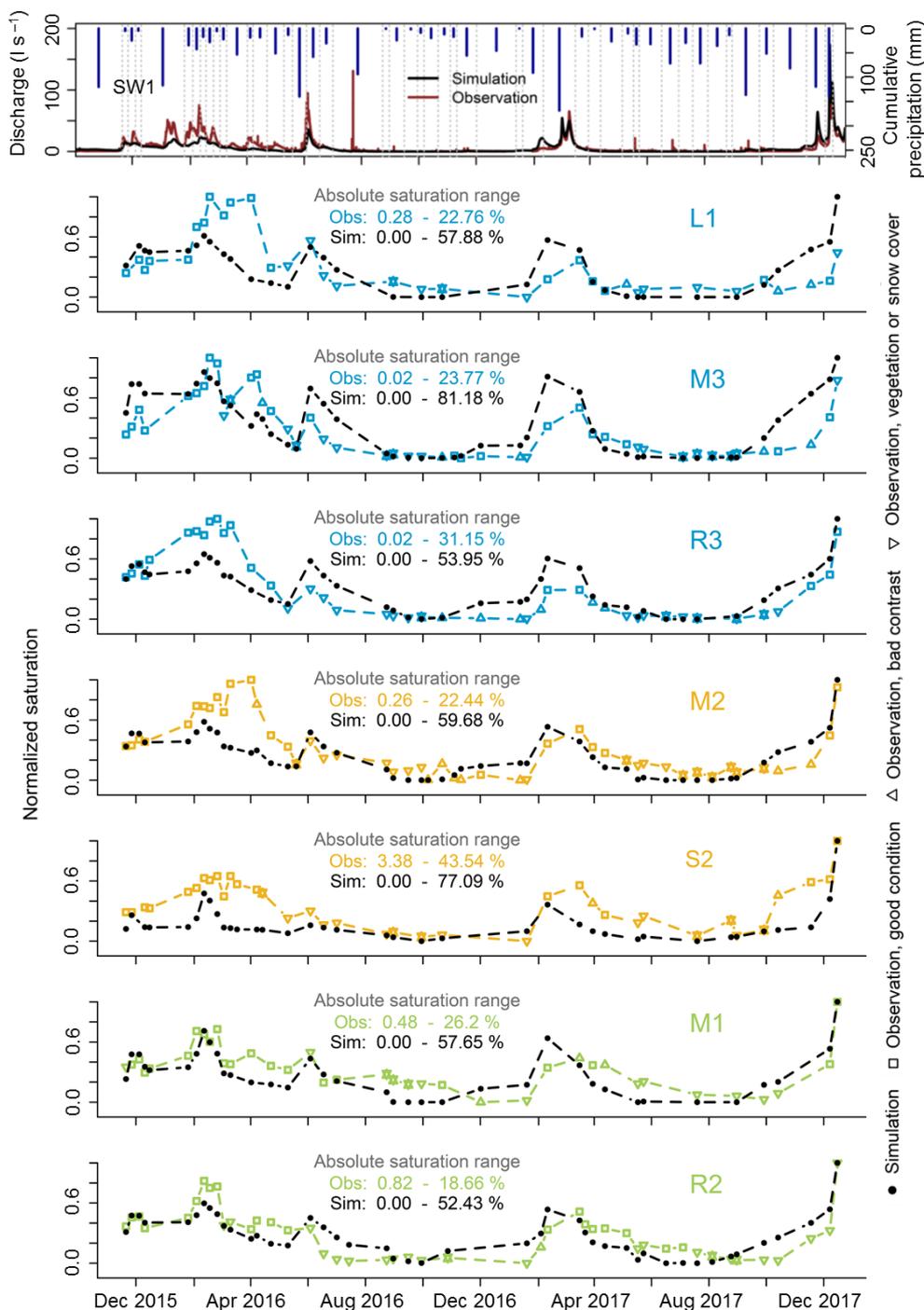
Figure 4: Time series of observed and simulated surface saturation in the seven investigated riparian areas. Surface saturation is normalized to the minimum and maximum amount of saturation that was observed and simulated in the individual areas, respectively. Observations that were derived from TIR images with a poor temperature contrast or with influences of vegetation and snow cover are deemed less reliable. Cumulative precipitation between the measurement dates (grey dashed lines) and discharge at catchment outlet SW1 are shown in the top panel for facilitating the comparison to precipitation and flow conditions.
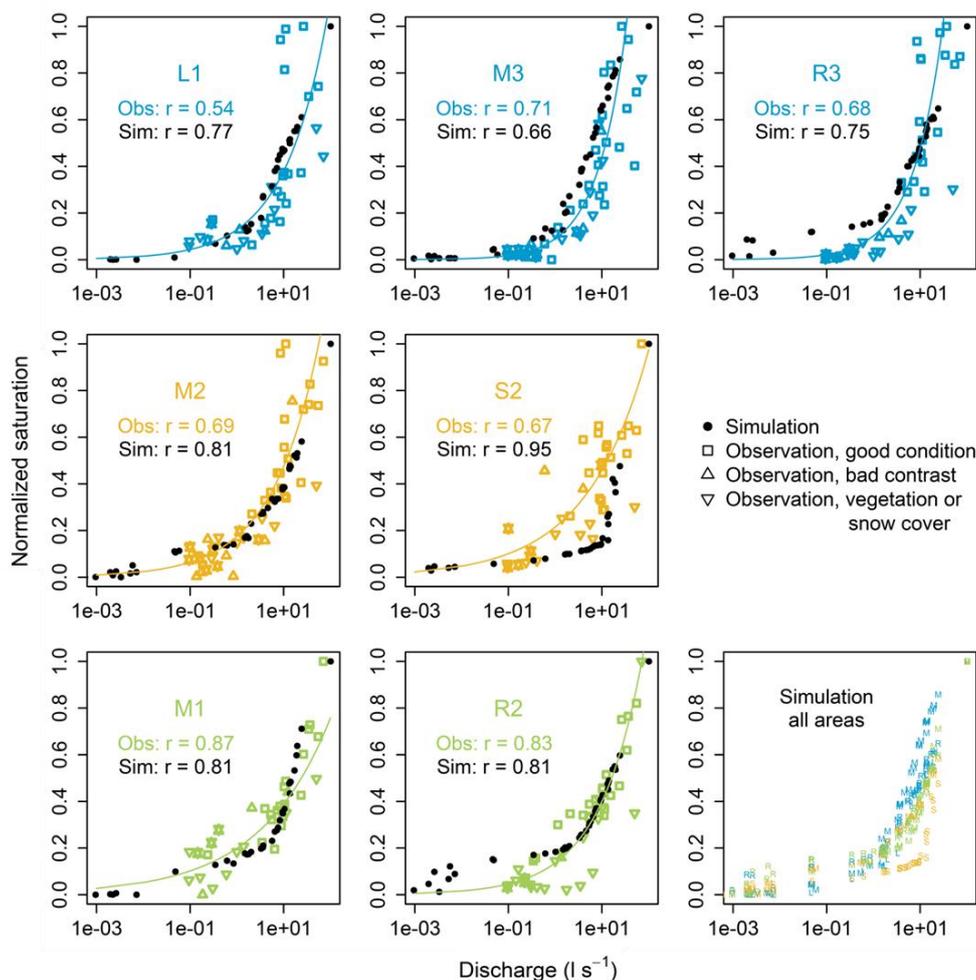
Figure 5: Observed and simulated relationships and Pearson correlations between normalized surface saturation and discharge at the catchment outlet SW1 for the seven investigated riparian areas. Observations that were derived from TIR images with a poor temperature contrast or with influences of vegetation and snow cover are deemed less reliable. Solid lines are power law curves
5 **fitted to the observation data, excluding data taken during rainfall or rising discharge. For facilitating the comparison between the seven areas, the panel on the bottom right contains the simulated data points from all seven areas and the area affiliation is indicated with the respective colour and letter.**

4.4 Spatial patterns of surface saturation

10 The realism of simulated patterns of surface saturation was evaluated for each riparian area by visually comparing the surface saturation frequency maps obtained from the simulations and observations (Fig. 6). The model captured the location of the stream and the locations that intermittently became surface saturated well for most of the seven investigated areas. For example, both observation and simulation showed that only the right side of the stream became saturated in M1, that the riparian zone of the right streamside in M2 became saturated only in the upstream part, and that saturation mainly developed on the left

15 streamside in R3, surrounding some permanently dry areas next to the stream (Fig. 6). The only area with a clear mismatch between observed and simulated patterns of surface saturation was area L1, where surface saturation was simulated on the opposite streamside and at a clearly wrong position along the stream (upstream vs downstream).

The simulated surface saturation also reflected the observed saturation frequencies well. The simulation reproduced the general picture of more frequent surface saturation in the streambed than at the streamsides, but - as for the saturation patterns - simulated and observed frequencies corresponded better in some areas (e.g. S2, Fig. 6) than in others (e.g. R3, Fig. 6). For example, the observed frequency of surface saturation in the streambed was generally lower in the source areas (L1, M3, R3)

5 than in the mid- and downstream areas (M2, S2, M1, R2), while the simulated frequency of surface saturation in the streambed was more similar between the areas and particularly overestimated in L1 and R3.
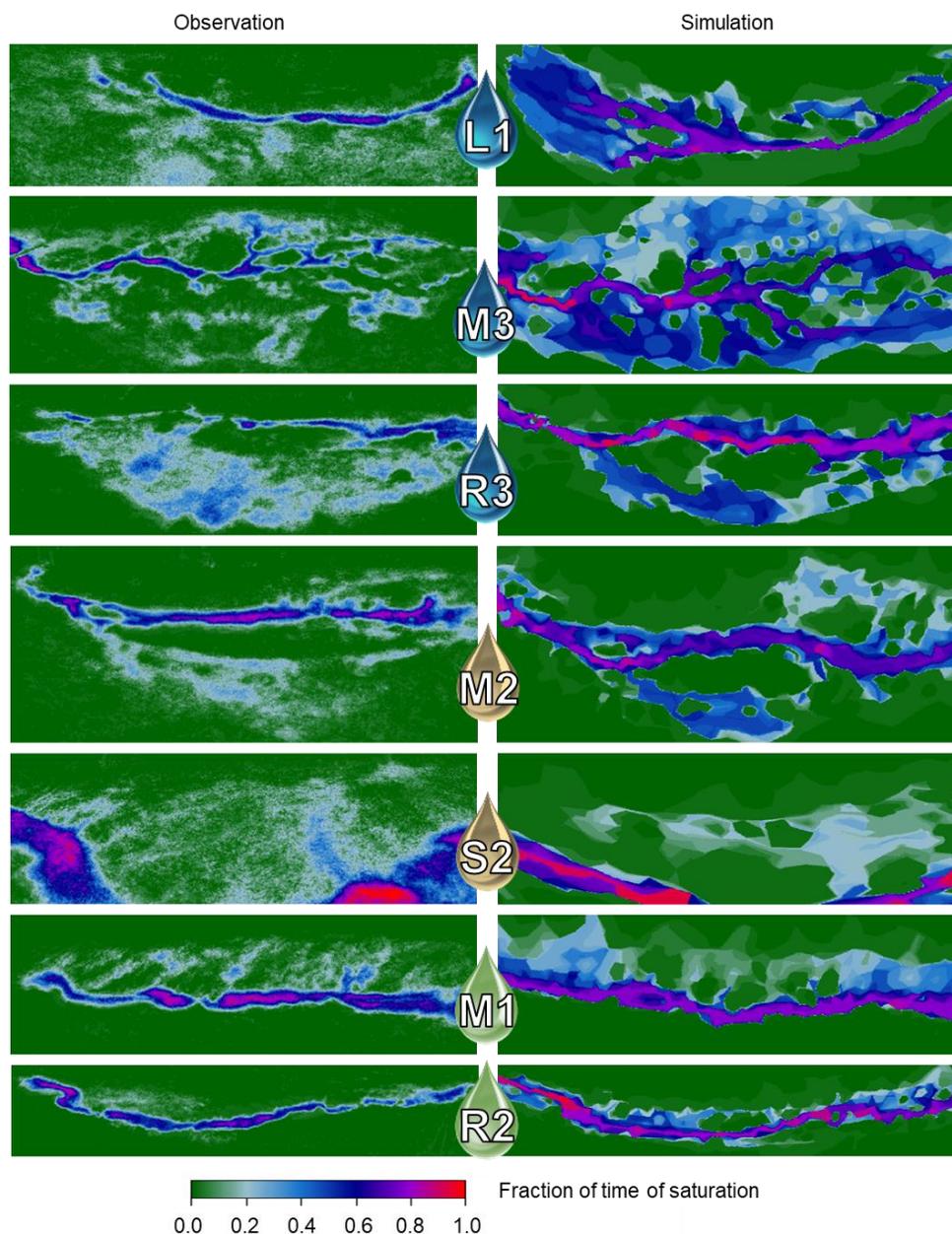
Figure 6: Observed (left) and simulated (right) frequencies of surface saturation in the seven investigated riparian areas. The maps
10 **were created by first counting how often the individual pixels were classified as saturated in the individual panoramic images and second normalizing the resulting frequency numbers by the total number of images analysed for the respective area.**

4.5 Simulated patterns and dynamics of surface saturation versus groundwater reaching the surface at catchment scale

Simulated surface saturation generally occurred only in the streambed and adjacent riparian zones (Fig. 7a). During the wettest conditions of the study period (winter 2017/2018), surface saturation also occurred as prolongation of the eastern stream branch into the hillslope above the source area R3. This simulated occurrence behaviour of surface saturation across the catchment is

5 in accordance with field evidence, where we observed surface saturation outside of the valley bottom only during very wet conditions or rain on snow events (cf. Section 2.2). The simulated patterns of where and how frequently groundwater reached the ground surface (Fig. 7b) proved to be very similar to the surface saturation frequency map of the catchment (Fig. 7a). The only obvious difference occurred in the area above the source area of the eastern stream branch (R3), with a smaller extent of groundwater reaching the surface than ~~extent of~~ surface saturation.
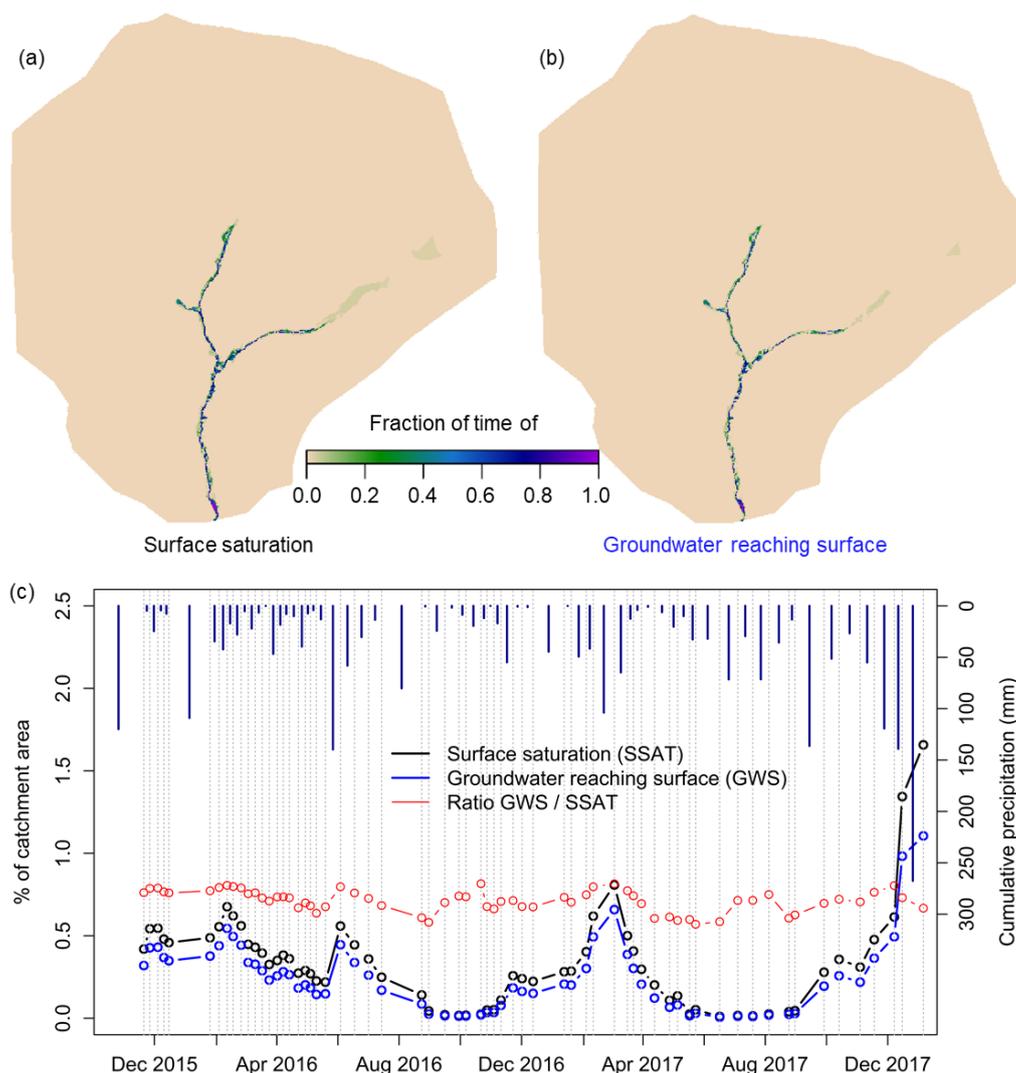
Figure 7: Simulated frequency maps (a, b) and time series of percentage (c) of surface saturation and groundwater reaching the surface in the Weierbach catchment. Precipitation is given as cumulative amounts between the observation dates (grey dashed lines).

The time series of simulated percentage of catchment area with surface saturation and groundwater reaching the surface revealed that the area where groundwater reached the surface was always smaller in extent than the surface saturated area, even after dry condition (Fig. 7c). The biggest absolute difference between the areal extent of surface saturation and groundwater reaching the surface was simulated during winter 2017/2018 (1.66 % vs 1.1 % of catchment area), where the

5 conditions were very wet with high discharge and high cumulative precipitation and where the difference in areal extent was also visible in the frequency maps (Fig. 7a and b). However, the ratio between the extent of groundwater reaching the surface and the extent of surface saturation was not exceptionally high during winter 2017/2018. Instead, the ratio ~~scattered~~ without a clear trend between 0.57 and 0.82 during the entire simulation period, apparently independent from the cumulative amount of precipitation or surface saturation.

10 **5 Discussion**

The aim of this study was to analyse the spatio-temporal variability of surface saturation within the Weierbach catchment, with a focus on the stream valleys and riparian zones. Even though simulated discharge, groundwater levels and soil moisture ~~showed some discrepancies to~~ observations in terms of absolute values, we would argue that the performance of the different time series at different locations was quite good for a model that was not calibrated and set up ~~rather homogenously~~ across the

15 catchment. While the model had some problems to reproduce soil moisture and groundwater levels during the dry conditions at hillslopes and plateau, the simulated time series matched the observations especially well in the riparian zone and vicinity. This gives us confidence that the model setup was valid for evaluating and analysing the spatio-temporal dynamics of surface saturation and its intra-catchment variability.

5.1 Temporal dynamics of surface saturation

20 The model reproduced the observed long-term dynamics of surface saturation over different seasons and wetness conditions well. Our study goes beyond previous works that compared the simulation of surface saturation dynamics with observations (e.g. Ali et al., 2014; Birkel et al., 2010; Glaser et al., 2016; Mengistu and Spence, 2016) by relying on a longer study period and a ~~higher~~ number of observations in time. This allowed us to analyse and compare various hydrological conditions and the dynamic transition between them over all seasons with a ~~frequent~~ number of observations. Moreover, we accounted for spatial

25 variability of saturated area dynamics within the catchment. Unlike the various quasi dynamic wetness indices presented in Ali et al. (2014), which could not satisfyingly reproduce the spatio-temporal variability of connected surface saturation observed in a catchment in the Scottish Highlands, our model reproduced the distributed dynamics of surface saturation well, without clear ~~performance~~ differences for different wetness conditions.

Simulations and observations showed both that the temporal dynamics of surface saturation were mostly consistent across the

30 catchment. Moreover, our simulations showed that the spatio-temporal development of surface saturation was very similar to the spatio-temporal dynamics of groundwater reaching the surface (cf. Fig. 7). This suggests that the generation of surface saturation in the Weierbach catchment is largely driven by the synchronous exfiltration of groundwater in topographic depressions. Antonelli et al. (2019) drew consistent conclusions based on a statistical analysis of the observation data.

5.2 Relation between surface saturation and discharge

35 We found that the observed and simulated relationships between surface saturation and discharge resembled power law relationships (cf. Fig. 5). This is consistent with earlier studies that showed power law relationships between contiguous connected surface saturated areas and discharge (Mengistu and Spence, 2016; Weill et al., 2013). In contrast to these studies, we did not observe hysteretic loops in the relationship between saturation and ~~high~~ streamflow. Nonetheless, the scatter in the observed discharge – surface saturation relationships might indicate that the development of surface saturation in the

Weierbach catchment follows hysteretic loops, but that the hysteresis was not resolved with the available temporal resolution of the observations. For example, it is likely that surface saturation evolved in the riparian areas during high flow conditions and persisted on the ground surface during decreasing streamflow due to restricted infiltration capacities of the riparian soil (cf. Antonelli et al., 2019).

5   The lack of such a hysteretic process in the simulation could explain why the model showed the tendency for less persistent and faster contracting surface saturation. It may also explain why the simulated saturation dynamics differed less between the different investigated areas than the observed dynamics. It is likely that the observed saturation dynamics were not synchronous between the different areas due to a less persistent (and thus hysteretic) generation of surface saturation in the relatively narrow riparian areas without perennial springs (M1 and R2) compared to the wider riparian areas with perennial springs (cf.

10   observation of less persistent saturation in M1 and R2 during February and April 2016, Fig. 4). The model, instead, simulated a non-hysteretic saturation behaviour for all investigated riparian areas, which resulted in a better fit between simulated and observed dynamics in the areas M1 and R2 compared to the other areas.

    At the same time, it might also be that the simulated relationship between saturation and discharge was correct in all riparian areas and that the scattering of the observation data did not result from hysteretic behaviour, but from uncertainties in the TIR

15   methodology. A good argument for a correct simulation of the discharge – surface saturation relationship is that not only simulated saturation but also simulated discharge seemed to be less persistent and to decrease and increase earlier than it was observed. In reality, the scatter of the observation data is likely related to both measurement uncertainties and hysteretic aspects and a future study with higher temporal resolution of field observations and corresponding simulation output could further analyse this.

20   Independently from the question on hysteretic loops, we found that the discharge – surface saturation relationships somewhat differed between the different areas. We could connect the main differences to different topographical and morphological features, yet we cannot decipher why the main controlling feature for the discharge – surface saturation relationship was different between observations (source areas vs non-source areas) and simulations (different stream branches, cf. Section 4.3). Nonetheless, our findings are in line with experimental studies that discussed that the relationships between baseflow discharge

25   and total extent of contributing saturated areas differ between catchments with different physiographic characteristics (e.g. Dunne et al., 1975; Latron and Gallart, 2007).

    By comparing our model results to the double logarithmic plot presented by Latron and Gallart (2007) (Figure 8), we could identify similar shape varieties of the discharge – surface saturation relationship for the different areas studied within the Weierbach catchment as observed for the different catchments presented in Latron and Gallart (2007). We cannot compare our

30   results directly with the results shown in Latron and Gallart (2007), since we evaluated absolute discharge and normalized saturation, while they evaluated connected saturated areas in percentage of catchment area, but discharge normalized to the catchment area. In order to facilitate the comparison and to connect the two plots (Fig. 8a, 8b), we show the simulated relationship between discharge and surface saturation of the entire Weierbach catchment in both plots, once with normalized discharge and absolute saturation (Fig. 8a), and once with absolute discharge and normalized saturation (Fig. 8b). The shape

35   of the relationship for the entire Weierbach catchment was nearly linear, similar to the relationship observed in the Can Vila catchment investigated by Latron and Gallart (2007) (Fig. 8a). The relationships of the seven studied riparian areas differed from the catchment relationship and between each other (Fig. 8b). For example, area S2 and M1 showed a convex shape similar to the observations in the Vermont W2 catchment made by Dunne et al. (1975), area M3 showed a rather concave shape similar to the relationships found for a sub-catchment of the Asker basin (Myrabø, 1986) and the Strengbach catchment (Latron, 1990),

40   area M2 showed a rather linear shape similar to the Can Vila catchment studied by Latron and Gallart (2007). This clearly shows that differences in the relationship between surface saturation and discharge do not only occur between different catchments, but that they also occur as intra-catchment variability.
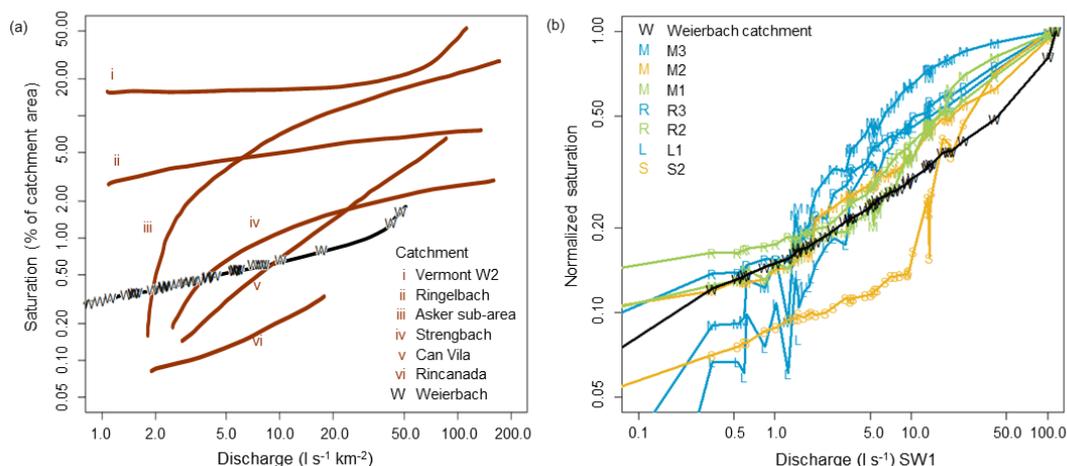
Figure 8: Simulated relationship between discharge and surface saturation of the entire Weierbach catchment (marked with W) in comparison to (a) the relationships observed in other catchments (Figure modified from Latron and Gallart (2007) and (b) the relationships simulated for the seven investigated riparian areas within the catchment. The presented relationships of the other
5 **catchments were investigated by i) Dunne et al. (1975), ii) Ambroise (1986), iii) Myrabø (Myrabø, 1986), iv) Latron (Latron, 1990), v) Latron and Gallart (2007), and vi) Martinez-Fernandez et al. (2005). Area affiliation for the investigated riparian areas of the Weierbach catchment is indicated with the respective colour and letter (cf. Fig. 4-6).**

5.3 Spatial patterns of surface saturation

10   The observed spatial patterns of surface saturation were reproduced ~~with~~ the simulations ~~in great detail~~ for most of the investigated areas. We attribute the successful simulation of the spatial patterns to microtopography (local topographical features with extents of centimetres to few metres) since i) microtopography described the main spatial variability between the seven investigated areas in the model setup and ii) we observed that small changes in the setup and resolution of the model mesh in the riparian zones changed some details of the simulated surface saturation patterns (Fig. S2, especially area M2, S2).

15   Therefore, we would like to stress that not only major topographic features of the catchment (e.g. hillslope shape, slope angle, valley width) but also its microtopography needs to be considered for identifying locations where surface saturation may occur. This may sound trivial and several studies have already pointed out the importance of microtopography for the simulation of different hydrological aspects such as hydraulic heads, hyporheic surface-subsurface water exchange, bank storage and overbank flooding, water quality of shallow groundwater systems and runoff generation (e.g. Aleina et al., 2015; Frei et al.,

20   2010; Käser et al., 2014; Van der Ploeg et al., 2012; Tang et al., 2018). Still, microtopography is not often considered in the simulation of surface saturation patterns.

When microtopography is not resolved ~~detailed~~ enough, it is more likely that the simulated surface water extends over a large area instead of ~~accumulating in~~ topographic depressions and thus ~~overrates~~ the extent of surface saturation. In this context it is interesting to note that there are studies that simulated maximum extents of surface saturation up to 80 % of the study area (Qu

25   and Duffy, 2007; Weill et al., 2013), while field observations have only ~~reached~~ maximum extents up to 25 % - 50 % of catchment area (Ali et al., 2014; Birkel et al., 2010; Dunne et al., 1975; Mengistu and Spence, 2016) and often ~~show~~ maximum extents around 10 % (Ambroise, 2016; Grabs et al., 2009; Güntner et al., 2004; Latron and Gallart, 2007; Tanaka et al., 1988). Microtopography might partly explain this discrepancy, even though the maximum extent of surface saturation certainly also depends on the climatic and physiographic conditions of the catchment and on the timing of the observations (e.g. baseflow

30   conditions vs storm events) and there are some studies that simulated similar or ~~less~~ maximum extent of surface saturation

than observed without considering the microtopography (e.g. Ali et al., 2014; Birkel et al., 2010; Grabs et al., 2009; Güntner et al., 2004; Mengistu and Spence, 2016).

In our study, the simulated maximum extent of surface saturation was 1.6 % of catchment area, which is small compared to other simulation studies, but matches the observation that surface saturation commonly only occurs within the riparian zone and streambed (extent of 1.2 %). Nonetheless, also our maximum saturation within the individual areas was overestimated compared to the observations (cf. Fig. 4). Besides the effect of microtopography, there are two other possible explanations for this. First, the largest simulated saturation occurred during winter 2017/2018, which is the same period where the model clearly overestimated discharge. This mismatch could partly explain the overestimation of saturation, assuming that the relationship between discharge and saturation was correctly captured with the model (cf. Section 5.2). Second, the overestimation of absolute saturation could result from different perspectives and extensions of model output and TIR images (cf. section 3.2, Fig. 6). The TIR images included parts of the hillslopes around the riparian zones, which were not included to the same extent in the extracted model images. Since the hillslopes normally remained unsaturated, the maximum possible amount of saturated pixels in the TIR images was thus lower than in the model images, while the minimum possible amount of saturation was not affected. This could also explain why overestimation of total amounts of saturation was different between the different areas.

Despite the importance of microtopography, the model results showed that microtopography alone was not sufficient to capture the spatial patterns of surface saturation correctly. The simulated patterns of surface saturation clearly did not match the observed patterns equally well in all seven investigated areas (cf. Fig. 6), although the topographical information source and mesh resolution was consistent for the simulated riparian areas. This means that there are additional factors that control the spatial patterns of surface saturation that were not accounted for in the simulations. Such a factor could for example be the structure of the subsurface, which was treated as being homogeneous between all investigated riparian areas in the simulations. In reality, the subsurface structure may locally differ to some degree, for example in the riparian area of the western stream branch (L1), where saturation was simulated at a clearly wrong side along the stream.

5.4 Frequency maps of surface saturation

The frequency maps of surface saturation combine information on when and where surface saturation occurs. We do not think that the exfiltration of subsurface water into local depressions (cf. Section 5.1 and 5.2) can fully explain the spatial variability of saturation frequencies that was observed and simulated satisfactorily within the different riparian areas (Fig. 6). Instead, we suppose that the differences in saturation frequency were controlled by additional water sources than exfiltrating groundwater, such as stream water or direct precipitation, and that the contribution of these additional water sources to surface saturation varied in space and time. For example, the lower frequencies of surface saturation observations at the streamsides compared to the streambed and the lower frequencies in the streambed of the source areas (L1, M3, R3) compared to the mid- and downstream areas (M2, S2, M1, R2) might reflect a lower and less frequent contribution of upstream water in these areas. The overestimation of simulated saturation frequencies in the streambed of R3 could thus indicate an overestimated upstream contribution due to simulating the stream extent too far upstream from the source area. Future work should analyse potential water sources and generation processes of surface saturation with a suitable model framework (cf. Partington et al., 2013; Weill et al., 2013) in order to complement the interpretation of the observation data and to identify the mixture of different water sources of surface saturation (e.g. stream water, exfiltrating subsurface water, ponding precipitation), how the sources might vary in space and time, and how this might reflect in the surface saturation frequencies.

6 Summary and conclusions

We explored the intra-catchment variability of surface saturation in the Weierbach catchment with joint observations and simulations. We showed that the model could reproduce the observed variability of the surface saturation characteristics

(dynamics, frequencies, patterns) with great detail, although the model setup was rather homogeneous and parameters were not calibrated at catchment scale. Our results demonstrated that a spatially distributed, physically-based, integrated hydrological model such as HGS is well-suited for reproducing and analysing the generation and development of surface saturation in space and time.

5 Based on the matches and mismatches between the simulation results and observations, we could identify some key factors controlling the surface saturation generation. The temporal occurrence of surface saturation was observed and simulated to be similar across the catchment, which we related – based on the simulation results – to a large influence of groundwater that reacts synchronous across the catchment. The spatial occurrence of the surface saturation differed between and within the seven investigated riparian areas, which we mainly could relate to the influence of microtopography. Furthermore, we

10 discussed that the full variability between the different areas and the mismatches between observations and simulation can only be explained with additional factors besides groundwater exfiltration and microtopography.

The spatially varying frequencies of surface saturation within the riparian areas indicated that there might be additional water sources than subsurface water that contribute to the generation of surface saturation. Since the model could reproduce the observed frequencies, the model can be used in a future study to analyse such a potential mixing of different water sources and

15 their variation in space and time. The observed differences between the investigated riparian areas with regard to the seasonal dynamics of saturation extension and contraction and the surface saturation – discharge relationship likely resulted from different morphological characteristics (width, existence of perennial springs) of the riparian areas. Although the model could not reproduce a varying hysteretic occurrence and persistence of surface saturation in the different investigated areas, also the simulation results demonstrated that the relationship between surface saturation and discharge can differ within a catchment

20 in the same manner as between catchments with different topographical and morphological conditions.

Data availability. Data underlying the study are property of the Luxembourg Institute of Science and Technology. They are available on request from the authors.

25 *Author contributions.* BG, LH and JK designed and directed the study. BG and MA planned and carried out the field work and processed the TIR images. BG set up the simulation and processed the model output. BG, MA, LH and JK discussed and interpreted the results. BG prepared the manuscript with contributions from JK and LH.

Competing interests. The authors declare that they have no conflict of interest.

30

Acknowledgments. We wish to thank Jean-Francois Iffly, Jérôme Juilleret, the Observatory for Climate and Environment of LIST, and the Administration des Services Techniques de l'Agriculture (ASTA) for the collection and provision of the hydrometrical and meteorological data. We acknowledge deployment of a trial version of AlgoMesh by HydroAlgorithmics Pty Ltd. Barbara Glaser thanks the Luxembourg National Research Fund (FNR) for funding within the framework of the FNR-

35 AFR Pathfinder project (ID 10189601). Marta Antonelli was funded by the European Union's Seventh Framework Programme for research, technological development, and demonstration under grant agreement no. 607150 (FP7-PEOPLE-2013-ITN – INTERFACES – Ecohydrological interfaces as critical hotspots for transformation of ecosystem exchange fluxes and bio-geochemical cycling).

References

40 Ala-aho, P., Rossi, P. M., Isokangas, E. and Kløve, B.: Fully integrated surface–subsurface flow modelling of groundwater–lake interaction in an esker aquifer: Model verification with stable isotopes and airborne thermal imaging, J. Hydrol., 522, 391–406, doi:10.1016/j.jhydrol.2014.12.054, 2015.

Aleina, F. C., Runkle, B. R. K., Kleinen, T., Kutzbach, L., Schneider, J. and Brovkin, V.: Modeling micro-topographic controls on boreal peatland hydrology and methane fluxes, Bio, 12, 5689–5704, doi:10.5194/bg-12-5689-2015, 2015.

Ali, G., Birkel, C., Tetzlaff, D., Soulsby, C., Mcdonnell, J. J. and Tarolli, P.: A comparison of wetness indices for the prediction of observed connected saturated areas under contrasting conditions, Earth Surf. Process. Landforms, 39(3), 399–
5   413, doi:10.1002/esp.3506, 2014.

Allen, R. G., Pereira, L. S., Raes, D. and Smith, M.: Crop evapotranspiration (guidelines for computing crop water requirements), FAO Irrig. Drain. Pap., 56, 1998.

Ambroise, B.: Rôle hydrologique des surfaces saturées en eau dans le basin du Ringelbach à Soultzeren (Hautes-Vosges), France, in Recherches sur l'Environnement dans la Région, Actes du 1er Colloque Scientifique des Universités du Rhîn
10 Supérieur, edited by O. Rentz, J. Streith, and L. Ziliox, pp. 620–630, Université Louis Pasteur - Conseil de l'Europe, Strasbourg., 1986.

Ambroise, B.: Variable water-saturated areas and stream fl ow generation in the small Ringelbach catchment (Vosges Mountains , France): the master recession curve as an equilibrium curve for interactions between atmosphere , surface and ground waters, Hydrol. Process., 30, 3560–3577, doi:10.1002/hyp.10947, 2016.

15 Antonelli, M., Glaser, B., Teuling, R., Klaus, J. and Pfister, L.: Saturated areas through the lens: 1. Spatio-temporal variability of surface saturation documented through Thermal Infrared imagery, In preparation, 2019.

Birkel, C., Tetzlaff, D., Dunn, S. M. and Soulsby, C.: Towards a simple dynamic process conceptualization in rainfall – runoff models using multi-criteria calibration and tracers in temperate, upland catchments, Hydrol. Process., 24, 260–275, doi:10.1002/hyp.7478, 2010.

20 Carrer, G. E., Klaus, J. and Pfister, L.: Assessing the Catchment Storage Function Through a Dual-Storage Concept, Water Resour. Res., 55, 476–494, doi:10.1029/2018WR022856, 2019.

Davison, J. H., Hwang, H.-T., Sudicky, E. A., Mallia, D. V. and Lin, J. C.: Full Coupling Between the Atmosphere, Surface, and Subsurface for Integrated Hydrologic Simulation, J. Adv. Model. Earth Syst., 10, 43–53, doi:10.1002/2017MS001052, 2018.

25 Dunne, T., Moore, T. R. and Taylor, C. H.: Recognition and prediction of runoff-producing zones in humid regions, Hydrol. Sci. Bull., 20, 305–327, 1975.

Erler, A. R., Frey, S. K., Khader, O., Orgeville, M., Park, Y.-J., Hwang, H.-T., Lapen, D. R., Peltier, W. R. and Sudicky, E. A.: Simulating Climate Change Impacts on Surface Water Resources Within a Lake-Affected Region Using Regional Climate Projections, Water Resour. Res., 55, 130–155, doi:10.1029/2018WR024381, 2019.

30 Frei, S., Lischeid, G. and Fleckenstein, J. H.: Effects of micro-topography on surface-subsurface exchange and runoff generation in a virtual riparian wetland --- A modeling study, Adv. Water Resour., 33(11), 1388–1401, doi:10.1016/j.advwatres.2010.07.006, 2010.

Gburek, W. J. and Sharpley, A. N.: Hydrologic Controls on Phosphorus Loss from Upland Agricultural Watersheds, J. Environ. Qual., 27, 267–277, doi:10.2134/jeq1998.00472425002700020005x, 1998.

35 Glaser, B., Klaus, J., Frei, S., Frentress, J., Pfister, L. and Hopp, L.: On the value of surface saturated area dynamics mapped with thermal infrared imagery for modeling the hillslope-riparian-stream continuum, Water Resour. Res., 52, 8317–8342, doi:10.1002/2015WR018414, 2016.

Glaser, B., Antonelli, M., Chini, M., Pfister, L. and Klaus, J.: Technical note: Mapping surface-saturation dynamics with thermal infrared imagery, Hydrol. Earth Syst. Sci., 22(11), 5987–6003, doi:10.5194/hess-22-5987-2018, 2018.

40 Glaser, B., Jackisch, C., Hopp, L. and Klaus, J.: How meaningful are plot-scale observations and simulations of preferential flow for catchment models ?, Vadose Zo. J., doi:10.2136/vzj2018.08.0146, 2019.

Gourdol, L., Clément, R., Juilleret, J., Pfister, L. and Hissler, C.: Large-scale ERT surveys for investigating shallow regolith properties and architecture, Hydrol. Earth Syst. Sci. Discuss., 1–39, doi:10.5194/hess-2018-519, 2018.

Grabs, T., Seibert, J., Bishop, K. and Laudon, H.: Modeling spatial patterns of saturated areas: A comparison of the topographic wetness index and a dynamic distributed model, J. Hydrol., 373(1-2), 15–23, doi:10.1016/j.jhydrol.2009.03.031, 2009.

Güntner, A., Seibert, J. and Uhlenbrook, S.: Modeling spatial patterns of saturated areas: An evaluation of different terrain indices, Water Resour. Res., 40, W05114, doi:10.1029/2003WR002864, 2004.

Gupta, H. V, Kling, H., Yilmaz, K. K. and Martinez, G. F.: Decomposition of the mean squared error and NSE performance criteria : Implications for improving hydrological modelling, J. Hydrol., 377, 80–91, doi:10.1016/j.jhydrol.2009.08.003, 2009.

Juilleret, J., Iffly, J. F., Pfister, L. and Hissler, C.: Remarkable Pleistocene periglacial slope deposits in Luxembourg (Oesling): pedological implication and geosite potential, Bull. la Société des Nat. Luxemb., 112(1), 125–130 [online] Available from: http://www.snl.lu/publications/bulletin/SNL_2011_112_125_130.pdf, 2011.

Käser, D., Graf, T., Cochand, F., McLaren, R., Therrien, R. and Brunner, P.: Channel Representation in Physically Based Models Coupling Groundwater and Surface Water : Pitfalls and How to Avoid Them, Groundwater, 52(6), 827–836, doi:10.1111/gwat.12143, 2014.

Kristensen, K. J. and Jensen, S. E.: A model for estimating actual evapotranspiration from potential evapotranspiration, Nord. Hydrol., 6(3), 170–188, doi:10.2166/nh.1975.012, 1975.

Latron, J.: Caractérisation géomorphologique et hydrologique du bassin versant versant du Strengbach (Aubure), Université Louis Pasteur, Strasbourg I., 1990.

Latron, J. and Gallart, F.: Seasonal dynamics of runoff-contributing areas in a small mediterranean research catchment (Vallcebre, Eastern Pyrenees), J. Hydrol., 335(1-2), 194–206, doi:10.1016/j.jhydrol.2006.11.012, 2007.

Martínez Fernández, J., Ceballos Barbancho, A., Morán Tejeda, C., Casado Ledesma, S. and Hernández Santana, V.: Procesos hidrológicos en una cuenca forestal del Sistema Central: Cuenca experimental de Rinconada, Cuad. Investig. Geográfica, 31, 7–25 [online] Available from: https://dialnet.unirioja.es/servlet/articulo?codigo=1975892, 2005.

Martínez-Carreras, N., Hissler, C., Gourdol, L., Klaus, J., Juilleret, J., Iffly, J. F. and Pfister, L.: Storage controls on the generation of double peak hydrographs in a forested headwater catchment, J. Hydrol., 543, 255–269, doi:10.1016/j.jhydrol.2016.10.004, 2016.

Megahan, W. F. and King, P. N.: Identification of critical areas on forest lands for control of nonpoint sources of pollution, Environ. Manage., 9(1), 7–17, doi:10.1007/BF01871440, 1985.

Mengistu, S. G. and Spence, C.: Testing the ability of a semidistributed hydrological model to simulate contributing area, Water Resour. Res., 52, 4399–4415, doi:10.1002/2016WR018760, 2016.

Moragues-Quiroga, C., Juilleret, J., Gourdol, L., Pelt, E., Perrone, T., Aubert, a., Morvan, G., Chabaux, F., Legout, a., Stille, P. and Hissler, C.: Genesis and evolution of regoliths: Evidence from trace and major elements and Sr-Nd-Pb-U isotopes, Catena, 149, 185–198, doi:10.1016/j.catena.2016.09.015, 2017.

Munz, M., Oswald, S. E. and Schmidt, C.: Coupled Long-Term Simulation of Reach-Scale Water and Heat Fluxes Across the River-Groundwater Interface for Retrieving Hyporheic Residence Times and Temperature Dynamics, Water Resour. Res., (53), 8900–8924, doi:10.1002/2017WR020667, 2017.

Myrabø, S.: Runoff Studies in a Small Catchment, Nord. Hydrol., 17, 335–346, doi:10.2166/nh.1986.0025, 1986.

Nasta, P., Boaga, J., Deiana, R., Cassiani, G. and Romano, N.: Comparing ERT- and scaling-based approaches to parameterize soil hydraulic properties for spatially distributed model applications, Adv. Water Resour., 126, 155–167, doi:10.1016/j.advwatres.2019.02.014, 2019.

Nippgen, F., McGlynn, B. L. and Emanuel, R. E.: Water Resources Research, Water Resour. Res., 51, 4550–4573, doi:10.1002/2014WR016719.Received, 2015.

Ogden, F. L. and Watts, B. a.: Saturated area formation on nonconvergent hillslope topography with shallow soils: A numerical investigation, Water Resour. Res., 36(7), 1795, doi:10.1029/2000WR900091, 2000.

Partington, D., Brunner, P., Frei, S., Simmons, C. T., Werner, A. D., Therrien, R., Maier, H. R., Dandy, G. C. and Fleckenstein, J. H.: Interpreting streamflow generation mechanisms from integrated surface-subsurface flow models of a riparian wetland and catchment, Water Resour. Res., 49(9), 5501–5519, doi:10.1002/wrcr.20405, 2013.

Pfister, L., McDonnell, J. J., Hissler, C. and Hoffmann, L.: Ground-based thermal imagery as a simple, practical tool for
5 mapping saturated area connectivity and dynamics, Hydrol. Process., 24(21), 3123–3132, doi:10.1002/hyp.7840, 2010.

Van der Ploeg, M. J., Appels, W. M., Cirkel, D. G., Oosterwoud, M. R., Witte, J.-P. M. and Van der Zee, S. E. A. T. M.: Microtopography as a Driving Mechanism for Ecohydrological Processes in Shallow Groundwater Systems, Vadose Zo. J., 11(3), doi:10.2136/vzj2011.0098, 2012.

Qu, Y. and Duffy, C. J.: A semidiscrete finite volume formulation for multiprocess watershed simulation, Water Resour.
10 Res., 43(8), 1–18, doi:10.1029/2006WR005752, 2007.

Reaney, S. M., Bracken, L. J. and Kirkby, M. J.: The importance of surface controls on overland flow connectivity in semi-arid environments: Results from a numerical experimental approach, Hydrol. Process., 28(4), 2116–2128, doi:10.1002/hyp.9769, 2014.

Scaini, A., Audebert, M., Hissler, C., Fenicia, F., Gourdol, L., Pfister, L. and Beven, K. J.: Velocity and celerity dynamics at
15 plot scale inferred from artificial tracing experiments and time-lapse ERT, J. Hydrol., 546, 28–43, doi:10.1016/j.jhydrol.2016.12.035, 2017.

Schilling, O. S., Gerber, C., Partington, D. J., Purtschert, R., Brennwald, M. S., Kipfer, R., Hunkeler, D. and Brunner, P.: Advancing Physically-Based Flow Simulations of Alluvial Systems Through Atmospheric Noble Gases and the Novel 37Ar Tracer Method, Water Resour. Res., 53, 10,465–10,490, doi:10.1002/2017WR020754, 2017.

20 Sebben, M. L., Werner, A. D., Liggett, J. E., Partington, D. and Simmons, C. T.: On the testing of fully integrated surface – subsurface hydrological models, Hydrol. Process., 27, 1276–1285, doi:10.1002/hyp.9630, 2013.

Silasari, R., Parajka, J., Ressl, C., Strauss, P. and Blöschl, G.: Potential of time-lapse photography for identifying saturation area dynamics on agricultural hillslopes, Hydrol. Process., 1–18, doi:10.1002/hyp.11272, 2017.

Tanaka, T., Yasuhara, M., Sakai, H. and Marui, A.: The Hachioji experimental basin study -- storm runoff processes and the
25 mechanism of its generation, J. Hydrol., 102, 139–164, 1988.

Tang, Q., Schilling, O. S., Kurtz, W., Brunner, P., Vereecken, H. and Hendricks Franssen, H.-J.: Simulating Flood-Induced Riverbed Transience Using Unmanned Aerial Vehicles , Physically Based Hydrological Modeling, and the Ensemble Kalman Filter, Water Resour. Res., (54), 9342–9363, doi:10.1029/2018WR023067, 2018.

Weill, S., Altissimo, M., Cassiani, G., Deiana, R., Marani, M. and Putti, M.: Saturated area dynamics and streamflow
30 generation from coupled surface-subsurface simulations and field observations, Adv. Water Resour., 59, 196–208, doi:10.1016/j.advwatres.2013.06.007, 2013.